Chemical Engineering Journal 149 (2009) 162–172

Contents lists available at ScienceDirect

Chemical Engineering Journal

journal homepage: www.elsevier.com/locate/cej

Application of CFD modelling to investigate fluidized limestone reactors for the remediation of acidic drainage waters

Rupa Vuthaluru[a], Moses Tade[a], Hari Vuthaluru[a,*], Yuri Tsvetnenko[b], Louis Evans[b], Jason Milne[b]

[a] Curtin University of Technology, Department of Chemical Engineering, GPO Box U198, Western Australia 6845, Australia
[b] Curtin University of Technology, Centre for Sustainable Mine Lakes, GPO Box U198, Western Australia 6845, Australia

ARTICLE INFO

Article history:
Received 12 May 2008
Received in revised form 14 October 2008
Accepted 17 October 2008

Keywords:
CFD
Fluidized beds
Multiphase flow
Limestone reactors
Hydrodynamics

ABSTRACT

To improve the efficiency of limestone utilization within a conical reactor, fluidization behaviour of solid–liquid flow is investigated using Computational Fluid Dynamic (CFD) modelling tools. Three-dimensional, unsteady state simulations using the Granular Eulerian multiphase approach are performed to determine dynamic characteristics of limestone particles within the reactor. The effect of inflow rate of water and limestone loading on flow properties are studied in several conical fluidized limestone reactor (FLR) configurations including a proposed up-scaled model. The results are validated using available lab- and pilot-scale measurements.

To understand the influence of drag models on CFD modelling of FLRs, several widely used drag models (such as Gidaspow and Syamlal) available in literature are reviewed. Resulting hydrodynamics from such reviews are incorporated into the simulations, to extract the best suitable sub models. Results from such simulations are compared with lab-scale measurements to confirm the most suitable model parameters for testing the proposed (up-scaled) design of FLR. Experimentally validated Eulerian multiphase models formulated in the present work are of practical significance and highly useful for testing the scaling-up of limestone reactors.

1. Introduction

The acidic drainage water produced from coal mining can be used in mining operations or, following treatment, for beneficial end uses such as aquaculture. The Centre for Sustainable Mine Lakes (CSML) has undertaken research in the last four years on fluidized limestone reactors (FLR) for remediation of acidic waters. An innovative, low cost, pilot-scale fluidized limestone reactor was developed as a result of collaboration between the Centre for Sustainable Mine Lakes of Curtin University, Griffin Coal Mining Company and Wesfarmers Premier Coal companies in Western Australia.

In principle the FLR operates by injecting mine water to the base of a conical vessel filled with limestone. The influent water is injected using a pipe directed into the base of the container. The outlet of the cone is situated at the top end of the container (Fig. 1). Within FLR, water flows down under pressure within the influent pipe to the bottom of the vessel. At low flow rates, the limestone remains stationary at the base of the container and water flows upwards through the pores without moving the limestone. However, at higher inflow rates or in other words, when the drag force of flowing fluid exceeds gravity, particles are lifted and fluidization occurs. The acidic water will be neutralized if there is sufficient residence time and limestone within the container.

This technique is similar to systems used in Scandinavia and West Virginia, commonly referred to as Diversion Wells [1,2] and to re-circulating fluidized limestone reactors that are used in South Africa [3–5] and pulsating reactors that have been developed in USA [6,7]. As distinct from the single pass through the present FLR system, the latter systems have the added expense of either a re-circulating pump to re-input fines back into the reactor (South African design) or two treatment tanks through which the water is passed (US system). The major advantage of this system over other active treatment systems is that there are no mechanical parts required for mixing. This design feature, together with the use of limestone rather than more expensive neutralizing reagents, reduces the ongoing costs associated with the system.

The aim of the present work was to assist the design of a commercial sized FLR and to develop design guidelines for conical FLRs that efficiently utilize limestone using Computational Fluid Dynamic (CFD) tools. It is well known that the fluidization properties within the vessel vary with changes in dimensions of the reactor. To reduce limestone lost out of the reactor and maximise design efficiency further research was required to understand the

* Corresponding author.
E-mail address: h.vuthaluru@exchange.curtin.edu.au (H. Vuthaluru).

1385-8947/$ – see front matter © 2008 Elsevier B.V. All rights reserved.
doi:10.1016/j.cej.2008.10.014

Nomenclature

C_D	drag coefficient
d_l	diameter of the particles of solid l
D	diameter of particle (m)
D_0	bottom diameter of bed (m)
D_1	top diameter of bed (m)
e_{ss}	restitution of coefficient
$\vec{F}_{lift,s}$	solids lift force
$\vec{F}_s$	solids external body force
$\vec{F}_{vm,s}$	solids virtual mass force
g	acceleration due to gravity, 9.80665 (m/s^2)
$\vec{g}$	acceleration due to gravity
$g_{o,ls}$	radial distribution coefficient
h	height of the fluidized limestone reactor (m)
I_{2D}	2nd invariant of the deviatoric stress tensor
K	collision coefficient
$\dot{m}_{pq}$ and $\dot{m}_{ls}$	characterizes mass transfer from qth phase to pth phase and from liquid to solids
p	pressure shared by all phases
p_s	solids pressure
Q	Fluid flow rate (m^3/s)
Re	particle Reynolds number, $d\rho u/\mu$ (dimensionless)
Re$_s$	solids relative Reynolds number
S	surface area of particles (m^2)
u	superficial velocity (m/s)
u_e	superficial velocity of particle entrainment (m/s)
u_{ff}	superficial velocity at full fluidization (m/s)
u_{mf}	superficial velocity at minimum fluidization (m/s)
u_t	terminal free-falling velocity of particle (m/s)
$\vec{v}_{ls}$	liquid solids interphase velocity
$\vec{v}_q$	velocity of phase q
V	volume (m^3)

Greek letters

α_q	volume fraction of phase q
α_s	volume fraction of solids
$\alpha_{s,max}$	maximum packing limit
ε	voidage (dimensionless)
ϕ	sphericity of particle (dimensionless)
ϕ_{ls}	energy exchange between the lth fluid and sth solid
$\gamma_{\Theta s}$	collisional dissipation of energy
λ_s	solids bulk viscosity
μ	fluid viscosity, 0.000954 (kg/s/m) for water at 22 °C
μ_s	shear viscosity of solid phase
$v_{r,s}$	terminal velocity of solids
θ, α, β	angle, degree; cone flare, or apex, angle = 2 (cone side angle)
Θ_s	granular temperature
ρ	fluid density, 997.8 (kg/m^3) for water at 22 °C
ρ_s	density of solid particles (kg/m^3)
$\bar{\bar{\tau}}_s$	solids stress–strain tensor

dynamics of this system and develop design criteria. An improved understanding of the fluid dynamics was achieved through the development of a CFD model which simulates particle movement within the fluidized limestone reactor.

Prior to these conical FLRs, several cylindrical FLRs were trialled in the laboratory and in field applications, however, problems were experienced in obtaining uniform fluidization due to insufficient fluidization, channelling and inadequate bed expansion due to particle interlocking, etc. Preliminary laboratory and field applications

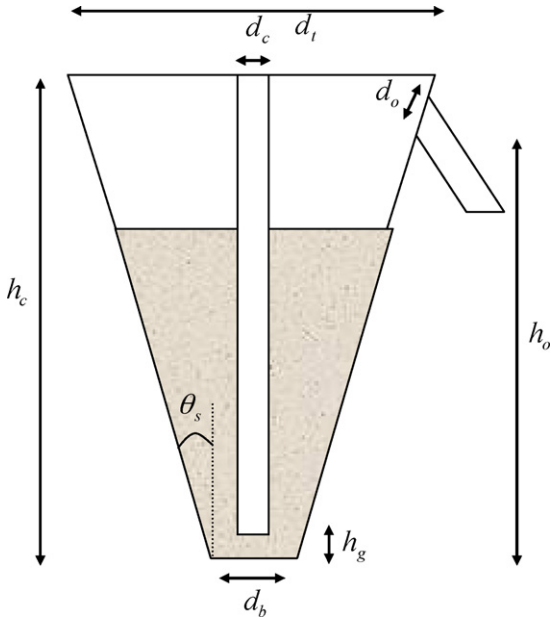

Fig. 1. Dimensional variables for FLRs. Cone 1 with static height = 533 mm. Chicken Creek Cone with static height = 2.4 m. Proposed Cone 1 with static height = 2.4 m. Proposed Cone 2 with static height = 2.52 m.

of a conical FLR proved to be a superior design. As the conical vessel diameter increases with height, the superficial vertical velocity changes accordingly. Therefore, particles with a greater range of size are able to remain in suspension within this vessel compared to a cylindrical container. This is desirable due to the variability in size range found in commercially available limestone.

Preliminary field trials with small conical vessels indicated that the fluidization dynamics vary with change in vessel dimensions, limestone loading and water flow rate and therefore up-scaling of these systems required further research. It was concluded that, if the fluidization properties are properly understood the system could be reliably up-scaled to ensure maximum efficiency in acidity remediation and metal removal.

1.1. Flow dynamics in FLRs

Fluidized beds are widely used in industry for mixing solid particles with gases or liquids. In most industrial applications, a fluidized bed consists of a bed of particulate solids through which there is an upward flow of fluid [8]. Within FLR, water flows down under pressure through a pipe from the bottom of the vessel. At low flow rates the limestone remains stationary at the base of the container and water flows upwards through the pores without moving the limestone. However, at higher inflow rates or in other words, when the drag force of flowing fluid exceeds gravity, particles are lifted and fluidization occurs. The acidic water will be neutralized if there is sufficient residence time and limestone within the container.

There are various methods available to calculate minimum fluidization velocity, v_{mf}. It should be noted that the bed pressure drop will be constant by the time minimum fluidization has been achieved. Also, the porosity of the bed, ε should be ε_{mf}, which is typically in the range of about 0.45–0.50.

One of the most popular theoretical approaches to calculate v_{mf} for spherical particles is by using Ergun equation [8,9]:

$$Ar = 150\frac{(1-\varepsilon)}{\varepsilon^3}\mathrm{Re}_{mf} + 1.75\frac{1}{\varepsilon^3}\mathrm{Re}_{mf}^2 \quad (1)$$

where,

$$Ar = \text{Archimedes Number} = \frac{D^3(\rho_p - \rho)\rho g}{\mu^2} \quad (2)$$

$$v_{mf} = \frac{\text{Re}_{mf}\mu}{\rho D} \quad (3)$$

Similarly, one of the most popular empirical correlations is Wen and Yu correlation [8,10], which is valid for spheres in the range $0.01 < \text{Re}_{mf} < 1000$ and can often be expressed as:

$$Ar = 1652\,\text{Re}_{mf} + 24.51\,\text{Re}_{mf}^2 \quad (4)$$

In homogeneous fluidization, the bed expands so that the porosity of the bed is uniform. This is the only mode of fluidization when the fluidization fluid is a liquid. For gases, it typically occurs for particles <50–100 μm. Initially, there is no increase in porosity as the fluid velocity increases and just before the actual v_{mf}, there may be slight increase in porosity as the particles rearranged to reduce friction. Large particles are usually fluidized with a smaller setup region (region after slight increase in ε until v_{mf}) while a more significant setup region exists for fine particles. Once fluidization occurs at v_{mf}, the porosity increases according to the equations [8,11]:

For slow flow,

$$v = \frac{(\rho_p - \rho)g\varepsilon^3}{K\mu(1-\varepsilon)S^2} \propto \frac{\varepsilon^3}{1-\varepsilon} \quad (5)$$

For higher flow,

$$v_f = v_o\varepsilon^n \quad (6)$$

where, typically: $n = 4.65$ for $\text{Re} < 0.3$ and $n = 2.4$ for $\text{Re} > 500$.

Hence, the drag force, minimum fluidization velocity and porosity or voidage in various sizes of FLRs were investigated with the help of CFD simulations using the commercial software package Fluent 6.3. Prior to constructing an up-scaled industrial scale FLR, CFD simulations were undertaken to gain confidence in its hydrodynamic behaviour.

2. Model description

In general, simulation of a fluidized bed system using Fluent is carried out in two steps. First, a three-dimensional computational mesh is generated using Gambit and then the bed hydrodynamic behaviour is simulated using an appropriate model within the multiphase flow models available in Fluent. Since the flow considered in the present work is a mixture of two different phases (liquid–solid), a multiphase model is needed. Currently there are two approaches available for the numerical calculation of multiphase flows: the Euler–Lagrange and the Euler–Euler approach. Since the flow is dense and the number of involved particles are more an Eulerian model with granular approach is selected.

The success of multiphase flows depends on the proper description of the solid stress and the interfacial forces. However, less effort was made to the study of the interfacial forces in the past. The interfacial forces include drag force; lift force and virtual mass force, etc. In coupling the equations of the two phases, due to the large difference in their densities, those forces other than drag force are less significant, and thus can be usually neglected [12]. Consequently, only drag force is considered.

CFD has been applied explicitly to liquid–solid and gas–solid fluidization in many numbers of cases. Comparatively less information is available regarding CFD modelling of the solids flow pattern in a liquid–solid fluidized beds [13–17] in contrast to the extensive knowledge of gas–solid fluidized beds [18–21] and bubble column reactors [22]. Most of these authors adopted an Eulerian–Eulerian approach, simplified the flow field as two-dimensional, assumed all particles to be spheres of uniform sizes, and adopted uniform flow as the upstream boundary condition. However, the approaches followed in these four studies differed in a number of other important respects.

While liquid fluidization may be simpler to model than gas-fluidized beds, since the hydrodynamics are more homogeneous, turbulence is much less of a factor, and the mismatch between the phase densities is reduced, the relevance of applying granular flow models may be questionable given the fact that collisions of particles may not actually occur when there is a liquid film separating adjacent particles. This is certainly a factor to be considered. However, Gidaspow and Lu [27] and Gidaspow et al. [23] suggested an

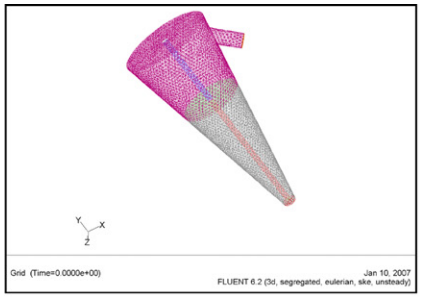

Cone 1 with Static Height = 533 mm

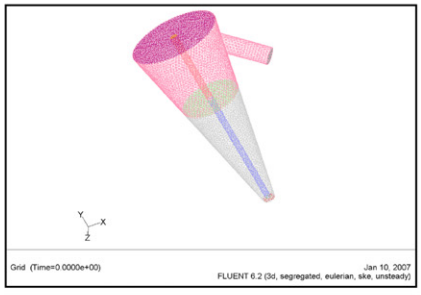

Chicken Creek Cone with Static Height = 2.4 m

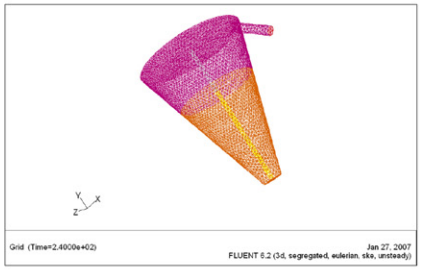

Proposed Cone1 with Static Height = 2.4 m

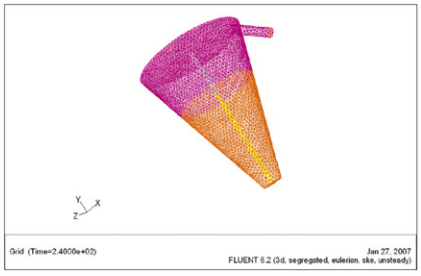

Proposed Cone2 with Static Height = 2.52 m

Fig. 2. Geometry and mesh of various cones constructed using Gambit.

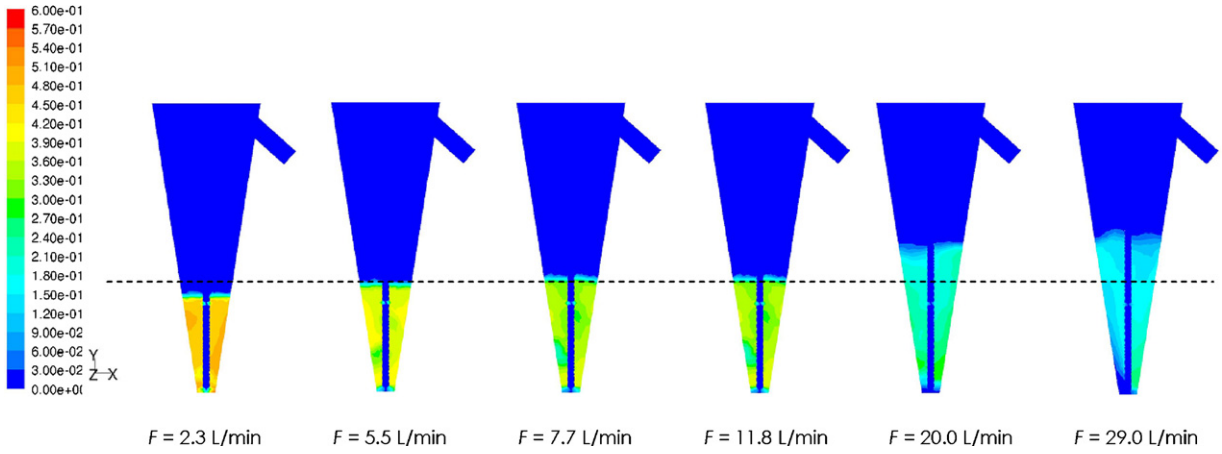

Fig. 3. Contours of volume fraction at various inflow rates of water at 4 min elapsed time for static height = 247 mm with 300 μm particle size, 0.45 initial voidage, Gidaspow drag model, Syamlal–O'Brien drag model and other key modeling parameters as described in Table 3.

"effective restitution coefficient" near 1. In the studies of Roy and Dudukovic [13] and Cheng and Zhu [14], the granular flow model was applied to liquid-fluidized beds, with coefficients of restitution less than one (implying inelastic collisions) and with no explicit consideration of whether or not the lack of collisions invalidates the approach and good agreement was claimed between predictions and experimental results. While some authors modelled the drag between the particles and continuous fluid based on experimentally determined Richardson–Zaki exponents for the various particle sizes, the others such as Panneerselvam et al. [16] aimed to evaluate the influence of interphase drag force models on the predictive capabilities of the numerical investigations.

It is worth noting the importance of the choice of drag models and their critical role in simulating gas–solid two-phase flows as well. Yasuna et al. [18] showed that the solution of their model was sensitive to the value of drag coefficients. Syamlal and O'Brien [19] suggested that the drag force correlations for fine particles should be corrected to account for the formation of clusters. Enwald et al. [20] found that the predictions based on different drag models were in good agreement with each other for dilute flow, but obviously different for the dense flow. Van Wachem et al. [21] noticed that flow predictions were not sensitive to the use of different solid stress models or radial distribution functions, as the different approaches were very similar in dense flow, but the application of different drag models significantly impacted the flow of the solid phase.

More or less, these results signify that an improper choice of drag models may yield inaccurate results or even lead to incorrect descriptions of gas–solid two-phase flows. By incorporating various drag models into the model, the present study is conducted with the aim of fully understanding the influence of the choice of drag models on simulations thereby laying a basis for the CFD modelling of fluidized limestone reactor systems.

Despite rigorous mathematical modelling of the associated physics, the drag models used in the simulations continue to be semi-empirical in nature. Therefore, it is crucial to use a drag model that correctly predicts the incipient or minimum fluidization conditions where the bed of particles is essentially in a state of suspension as a result of the balance between interfacial drag and body forces.

2.1. Gambit

Six different geometries of conical FLRs have been created and meshed using Gambit and exported to Fluent in order to study the bed expansion behaviour in liquid/solid flow. Fig. 1 shows the dimensional variables associated with conical FLR considered for the present work. The cones created are shown in Fig. 2, while the dimensions of each cone are reported in Table 1.

The three-dimensional spaces for all geometries were discretised in equally spaced tetrahedral grids for computational iterative calculation. Each mesh had a different number of grid cells depending on their sizes.

2.2. Fluent

In the present work, the Eulerian Granular Multiphase (EGM) was chosen to investigate the behaviour of FLRs. The closure models for granular multiphase flows, as solved by Fluent, for the general case of an *n*-phase flow are shown in Table 2. The EGM model was selected over other models because EGM includes granular kinetic theory to predict the pressure and viscosity of the solid phase. Both the solids pressure and viscosity are a function of granular temperature, the specific fluctuating energy of individual particles.

The drag correlation was chosen to be Gidaspow model [23] since the model to be developed is meant for simulating a dense fluidized bed [24]. However, several simulations were carried out using other drag models such as Syamlal–O'Brien (SO) and Wen–Yu. The SO drag model is based on measurements of terminal velocities of particles in fluidized or settling beds, with correlations which are a function of the volume fraction and relative Reynolds number [11]. The Wen–Yu model is appropriate to model dilute flow [10], where the volume fraction of solids is considerably lower than the fluid volume fraction. The Gidaspow drag model is a combination of the Wen–Yu model and the Ergun equation. The correlations used in each drag model and the key parameters used in simulations are presented in Tables 2 and 3.

3. Results and discussion

In general fluidization dynamics vary with change in vessel dimensions, particle loading (limestone) and fluid flow (water flow rate). Therefore to understand fluidization properties of the present system of conical FLRs and to up-scale these systems efficiently, a systematic study was carried out by investigating the above-mentioned parameters in several conical fluidized reactors, namely, Cone 1 (lab scale), Chicken Creek (pilot scale) and proposed scale-up (commercial scale). An important part of the study was to validate the model simulations with lab-scale FLR (Cone 1) experimental data and also to fine tune the simulations with the help of testing

Table 1
Dimensions of different conical shaped of FLRs.

Dimensions (mm)	Cone 1	Chicken Creek Cone	Proposed Cone 1	Proposed Cone 2
Top diameter, d_c	300	1370	2500	2680
Bottom diameter, d_b	50	230	460	460
Height, h_c	800	3650	4000	4040
Outflow pipe location, h_o	750	3400	3400	3400
Side angle θ_s	8.9	8.9	17.4	15.5
Outflow pipe diameter, d_o	50	283	283	283
Inflow pipe diameter, d_t	20	107	107	107
Inflow cross-sectional area (m^2)	3.14e−4	8.99e−3	8.99e−3	8.99e−3
Gap between tube and base, h_g	10	40	40	40

Table 2
Fluid–solid exchange coefficient of different drag models.

Syamlal–O'Brien [19]	Drag coefficient [25]	$C_D = \left(0.63 + \frac{4.8}{\sqrt{\mathrm{Re}_s/v_{r,s}}}\right)^2$
	Relative Re [11]	$\mathrm{Re}_s = \frac{\rho_l d_s \lvert\vec{v}_s - \vec{v}_l\rvert}{\mu_l}$
	Fluid–solid exchange coefficient	$K_{sl} = \frac{3\alpha_s\alpha_l\rho_l}{4v_{r,s}^2 d_s} C_D\left(\frac{\mathrm{Re}_s}{v_{r,s}}\right)\lvert\vec{v}_s - \vec{v}_l\rvert$
	Terminal velocity [26]	$v_{r,s} = 0.5(A - 0.06\,\mathrm{Re}_s + \sqrt{(0.06\,\mathrm{Re}_s)^2 + 0.12\,\mathrm{Re}_s(2B - A) + A^2})$ where, $A = \alpha_l^{4.14}$, $B = 0.8\alpha_l^{1.28}$, for $\alpha_l > 0.85$; $B = \alpha_l^{2.65}$, for $\alpha_l > 0.85$
Wen–Yu [10]	Drag coefficient	$C_D = \frac{24}{\alpha_l \mathrm{Re}_s}\left[1 + 0.15(\alpha_l\,\mathrm{Re}_s)^{0.687}\right]$
	Relative Re [11]	$\mathrm{Re}_s = \frac{\rho_l d_s \lvert\vec{v}_s - \vec{v}_l\rvert}{\mu_l}$
	Fluid–solid exchange coefficient	$K_{sl} = \frac{3}{4} C_D \frac{\alpha_s\alpha_l\rho_l\lvert\vec{v}_s - \vec{v}_l\rvert}{d_s}\alpha_l^{-2.65}$
Gidaspow, Wen and Yu, and Ergun [9,10,23]	Drag coefficient	$C_D = \frac{24}{\alpha_l \mathrm{Re}_s}\left[1 + 0.15(\alpha_l\,\mathrm{Re}_s)^{0.687}\right]$
	Relative Re [11]	$\mathrm{Re}_s = \frac{\rho_l d_s \lvert\vec{v}_s - \vec{v}_l\rvert}{\mu_l}$
	Fluid–solid exchange coefficient	$K_{sl} = \frac{3}{4} C_D \frac{\alpha_s\alpha_l\rho_l\lvert\vec{v}_s - \vec{v}_l\rvert}{d_s}\alpha_l^{-0.265}$, for $\alpha_l > 0.8$ $K_{sl} = 150\frac{\alpha_s(1-\alpha_l)\mu_l}{\alpha_l d_s^2} + 1.75\frac{\rho_l\alpha_s\lvert\vec{v}_s - \vec{v}_l\rvert}{d_s}$, for $\alpha_l > 0.8$

different drag models. Finally, validated model parameters were used to test an up-scaled design for its efficiency.

The minimum bed expansion and fluid velocity are influenced by the cone's top diameter, bottom diameter and therefore its flare angle. It is hypothesized that if the ratio of top diameter, bottom diameter and height are kept constant then fluidization dynamics should be similar in an up-scaled cone to that of the original cone.

In the design of FLR at Chicken Creek, this up scaling theory was followed, based on Cone 1, the small-scale laboratory design. Therefore it is logical to undertake the modelling of Cone 1 to start with and up-scale the model to Chicken Creek dimensions for the comparison of fluidization dynamics. Finally, the new proposed cone was simulated, based on the results of these two cones.

For the above-mentioned reasons, a significant part of this study was focused on simulating the Cone 1 fluidized limestone reactor (Cone 1 FLR) at different operating conditions such as different flow rates and static heights. Further more; validating Cone 1 model results with available experimental measurements was an important part of this study.

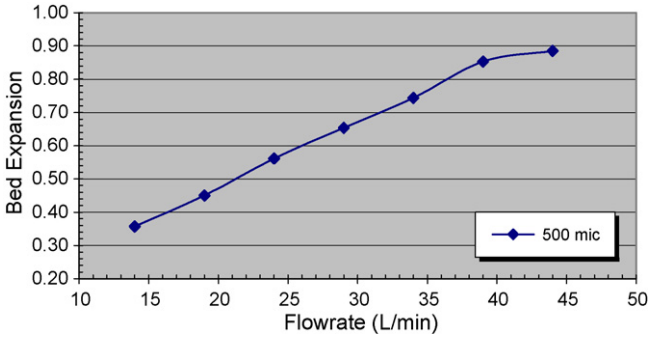

Fig. 4. Bed expansion for Cone 1 with 533 mm static height, 500 μm particles.

3.1. Study of bed expansion for Cone 1

Initial simulations were carried out using the following boundary conditions. The inflow rates of water considered are 14, 19, 24, 29, 34, 39 and 44 L/min with the particle size of 500 μm. The simulations used the Gidaspow correlation for drag coefficient model and the Syamlal–O'Brien correlation for kinetic granular viscosity.

The contours of volume fraction were observed carefully at various inflow rates of water after an elapsed time of 4 min to recognise the bed surface and estimate the fluidized bed height. An example of flow regime evolution and the contours of volume fraction are shown in Fig. 3. By using the contours of volume fraction, the static and fluidized heights were extracted and further utilized to estimate the bed expansion based on the equation given in Appendix

Table 3
Key parameters used in simulations.

Description	Value	Comment
Particle density	2500 kg/m^3	Limestone ($CaCO_3$)
Fluid density	998.2 kg/m^3	Water–liquid
Lateral boundary condition type	Wall	No-slip boundary condition
Inlet boundary condition type	Velocity inlet	Superficial fluid velocity
Outlet boundary condition type	Outflow	Fully developed flow
Granular bulk viscosity	Lun et al.	Default in Fluent
Frictional viscosity	None	Default in Fluent
Granular temperature	Algebraic	Default in Fluent
Solids pressure	Lun et al.	Default in Fluent
Radial distribution	Lun et al.	Default in Fluent
Elasticity modulus	Derived	Default in Fluent
Restitution coefficient	0.9	Default in Fluent
Packing limit	0.6	Fixed value

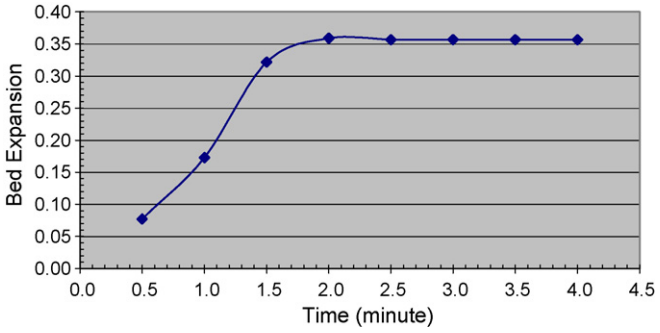

Fig. 5. Bed expansion as a function of time for Cone 1 with a flow rate of 14 L/min, 533 mm static height, 500 μm particles.

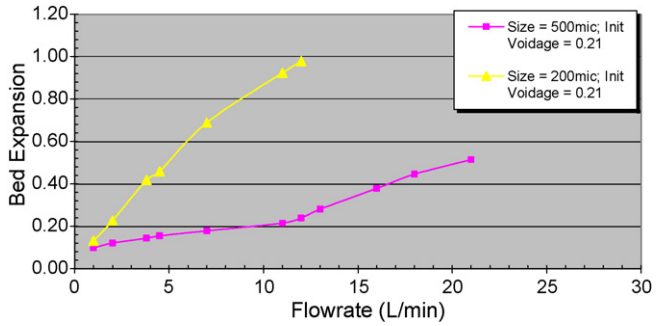

Fig. 6. Comparison of bed expansion for different particle sizes for Cone 1 with 533 mm static height.

A. It can be seen that the bed expansion increases linearly with the inflow rates of water (Fig. 4). The initial static height considered was 533 mm, which will occupy 8.24 L of the space in the reactor. Fig. 5 shows the bed expansion behaviour as a function of time. It can be inferred from the figure that the flow dynamics stabilize after 2.5 min. Depending on the dimensions of each cone the stabilization time varied from 2.5 to 3.5 min. Hence each set of simulations was carried out for at least 4 min.

Fig. 6 describes the behaviour of bed expansion for different limestone particle sizes as the aggregate. It can be inferred from the results that, as the limestone particle size decreases from 500 to 200 μm, the bed expands to a greater extent for all inflow rates of water. This behaviour is in line with the principle that finer particles will require less upward forces to lift up limestone particles and thus at the same water inflow rate, the bed will expand to a greater extent for 200 μm of limestone as compared to 500 μm. Even, for simulations using 200 μm, at water inflow rate of 13 L/min and above, some of the limestone particles have over flown at the outlet pipe, which is undesirable in industrial application. Therefore, it is difficult to measure bed expansion at these water inflow rates. This phenomenon is demonstrated in Fig. 7.

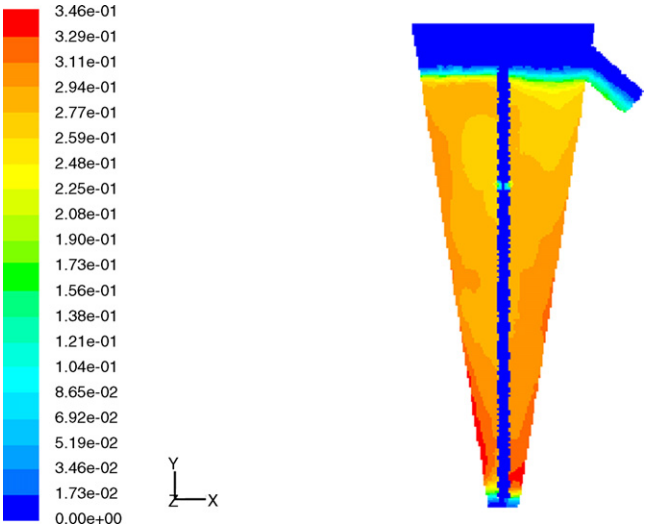

Fig. 7. Limestone chips overflow (flow rate 16 L/min; particle size = 200 μm; static height = 533 mm).

3.2. Study of bed expansion for Chicken Creek Cone

The Chicken Creek Cone is an up-scaled model of Cone 1. It is designed such that the base diameter, top diameter and height are 4.5 times the size of Cone 1. The inflow rates of water considered for this cone were 300, 350, 400, 450, 500 and 600 L/min with the particle size of 500 and 300 μm. The simulations used the Gidaspow correlation for the drag coefficient model and the Syamlal–O'Brien correlation for the kinetic granular viscosity while the other parameters were set constant. The initial static height was 2.40 m, occupying 757 L of the space in the reactor.

The results shown in Fig. 8 indicate that the same behaviour occurred for Chicken Creek Cone as compared with Cone 1 results in which the bed expansion is linearly proportional to inflow rates of water. Also, the bed expands to a greater extent for the simulation with 300 μm as compared to the one with 500 μm. Fig. 9 shows the bed expansion behaviour as a function of time. It can be inferred from the graph that the flow stabilizes after 3 min of simulation.

3.3. Validation of Cone 1 simulations with lab-scale experimental data

3.3.1. Experimental method

A re-circulating system of a prototype conical reactor Cone 1 was assembled and equipped with a water receiving tank to mea-

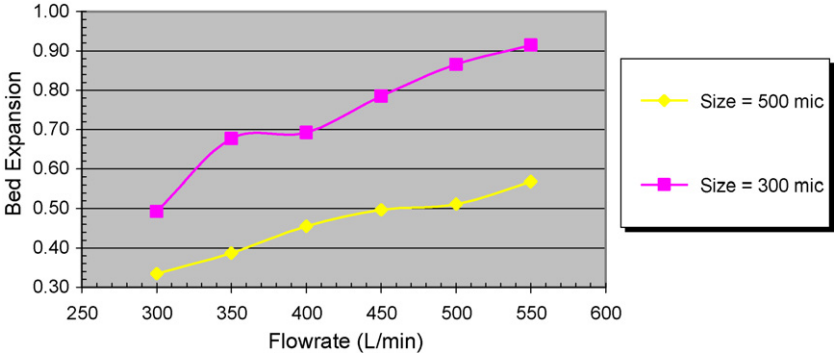

Fig. 8. Bed expansion for Chicken Creek Cone with 2.40 m static height, comparing different particle sizes of 500 and 300 μm.

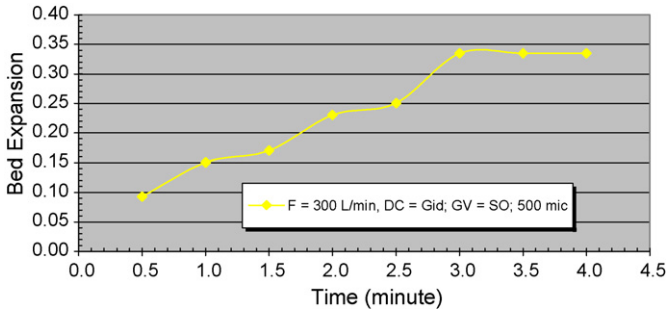

Fig. 9. Bed expansion as a function of time for Chicken Creek Cone with F = 300 L/min, 2.40 m static height, 500 μm particle size.

sure flow rate in the laboratory as shown in Fig. 10. This installation had been used to measure fluidization parameters at different solid loads and water inflow rates. The data obtained were compared with simulation results for validating and improving modelling results.

The cone was fabricated from polyvinyl chloride (PVC) sheeting, bent into a conical shape, with the dimensions of 800 mm high with 300 mm top diameter and 50 mm base diameter. The influent water was injected using a 20 mm pipe directed into the base of the container. The outlet of the cone consisted of a 50 mm diameter outlet situated at the top end of the container.

The experiments were conducted for static heights of 247, 410, 485 and 550 mm. The fluidized height was measured for various inflow rates of water in Cone 1. The limestone was screened for 500 μm (the mean particle size will be considerably lower than 500 μm) and used as the aggregate in all experiments. In the real industrial application, the limestone is supplied by either Lake Preston lime (68% between 0.125 and 0.5 mm), Lime Industries (93% between 0.125 and 0.5 mm) or Cook Industries (80% between 0.125 and 0.5 mm) is placed into the reactors and drainage water enters via a pipe with an open end at the base of the reactor.

Fig. 10. Experimental setup for Cone 1.

3.3.2. *Cone 1 with 247 mm static height*

Results showed that the fluidized height increases in response to an increase in inflow rates of water through the aggregate bed for both simulation as well as the experimental cases. Based on Figs. 11 and 12, it is evident that the fluidized heights and the bed expansions increase as the particle size increases. The simulations used the Gidaspow correlation for the drag model and the Syamlal–O'Brien correlation for the granular kinetic viscosity. The bed expansion average absolute errors, $|e|_{av}$ for 300, 400 and 500 μm models as compared to the experimental results as shown in Fig. 12 are 0.245, 0.717 and 0.684 respectively. Since 300 μm simulations gave the closest match, this mean particle size was used for other simulation runs.

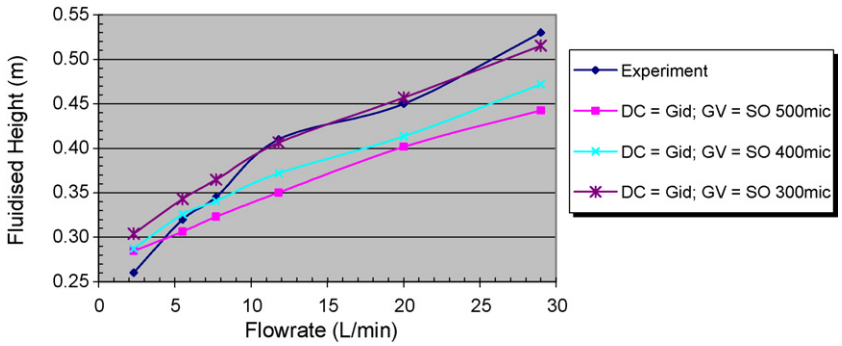

Fig. 11. Comparison of experimental and several model simulations of fluidized height for different particle sizes for Cone 1 with 247 mm static height, Gidaspow drag coefficient (DC) model, Syamlal–O'Brien granular viscosity (GV).

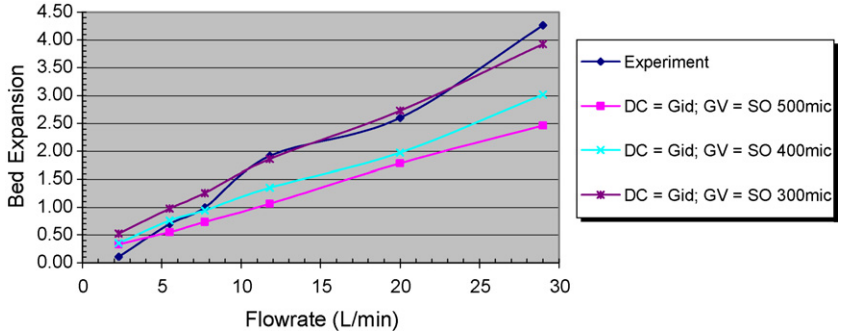

Fig. 12. Comparison of experimental and several model simulations of bed expansion for different particle sizes for Cone 1 with 247 mm static height (for legend see Fig. 11).

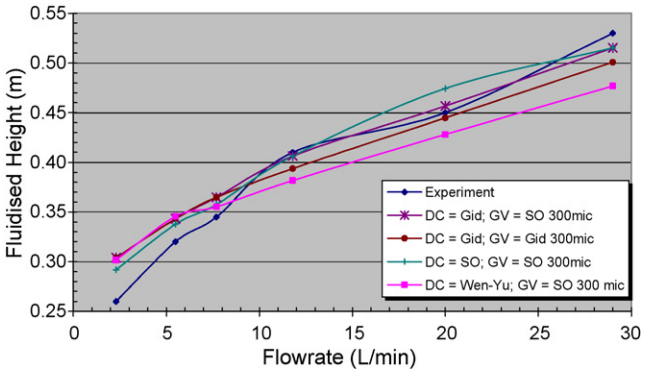

Fig. 13. Comparison of experimental and several model simulations of fluidized height for different drag coefficient models and granular kinetic viscosity models of Cone 1 with 247 mm static height, particle size of 300 μm (for legend see Fig. 11).

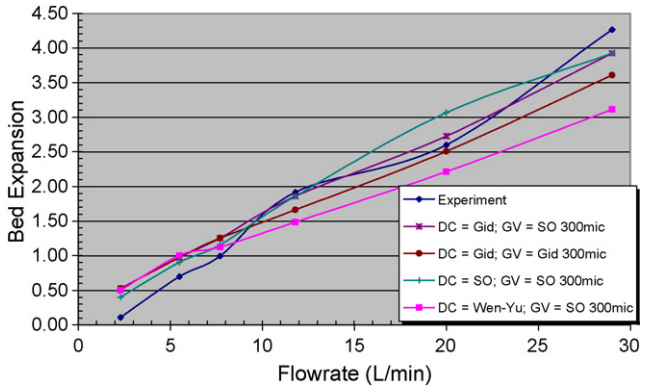

Fig. 14. Comparison of experimental and several model simulations of bed expansion for different drag coefficient models and granular kinetic viscosity models for Cone 1 with 247 mm static height, particle size of 300 μm (for legend see Fig. 11).

Next, several sets of simulations were carried out in order to compare different drag coefficient models and granular kinetic viscosity as shown in Figs. 13 and 14. When using the Syamlal and O'Brien model for the granular kinetic viscosity then the Gidaspow drag model lies in between Wen–Yu and Syamlal–O'Brien drag models, especially at higher water inflow rates. The $|e|_{av}$ of bed expansion for Gidaspow, Syamlal–O'Brien and Wen–Yu drag models as compared to the experimental results are 0.245, 0.254 and 0.466 respectively. Since the Gidaspow drag model simulations gave the closest match, this drag model was used as a basis for other simulations.

Rationally speaking, simulations using multiple particle size will resemble the real aggregate of limestone bed in the experiment. Therefore, investigations using mean particle size (either harmonic mean or arithmetic mean) were carried out to compare with n-phase of solids in which each phase will represent individual particle size of limestone (Fig. 15), using Mixture Model. The Mixture Model was used instead of EGM for multiple particle size simulations as the EGM model suffered computational instability in every simulation.

Then, the effect of varying the initial voidage of limestone aggregate was investigated. It can be noted that the simulations with 0.21 initial voidage although unrealistic gave a closer match to the experimental data (bed expansion $|e|_{av} = 0.245$) compare to the one with 0.45 initial voidage (bed expansion $|e|_{av} = 0.663$). The large deviation for 0.45 initial voidage model was contributed from higher water inflow rates while at lower rates, the model seems to match quite closely to the experiment.

Furthermore, the simulation results for the 200 μm model were also compared to the one with 300 μm of particle size with the same initial voidage of 0.45. Clearly, from Fig. 16, the bed expands

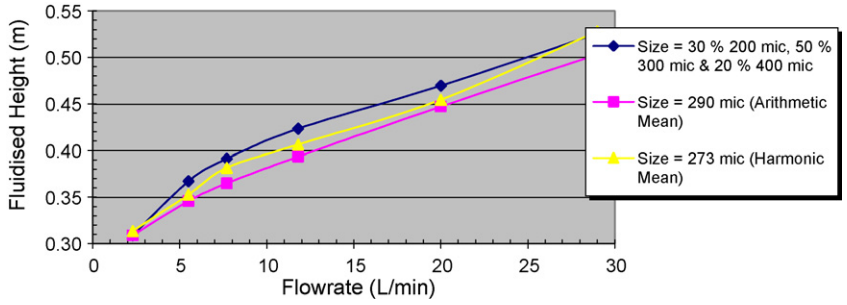

Fig. 15. Comparison of bed expansion for arithmetic and harmonic mean with multiple particle sizes for Cone 1 with 247 mm static height.

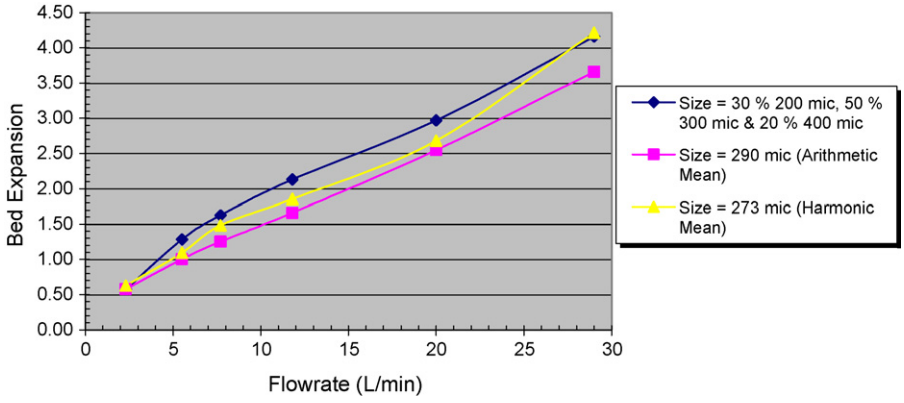

Fig. 16. Bed expansion for Cone 1 with 247 mm static height comparing different initial voidage and particle sizes.

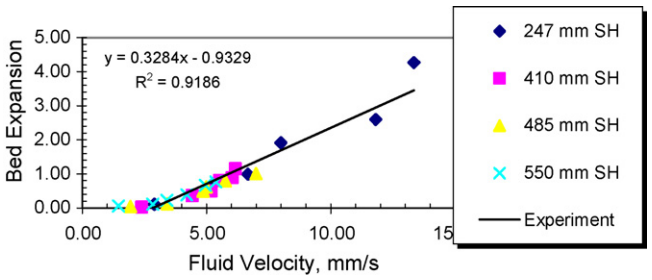

Fig. 17. Bed expansion vs. superficial fluid velocity for experimental result (SH—static height).

to a greater extent for the finer particle size simulation. The bed expansion $|e|_{av}$ for the 200 μm model was 0.425. Some of the possible reasons that lead to the large deviations at higher water inflow rates between experiment and model with particle size of 300 μm and initial voidage of 0.45 are:

- The experiments for a particular static height were done by continuously increasing the water inflow rates from one to the other without letting the fluidized aggregate to settle down first. While, for CFD simulation point of view, each simulation for a particular inflow rate of water was initialized by an assigned static volume. In other words, in the experiment, the previously fluidized aggregate might assist in overestimating the fluidized height for a higher water inflow rates.
- At higher rates, the attrition effect of limestone particles might be more apparent than at lower water inflow rates which will result in finer particles to be produced and thus higher fluidized height will occur.

Since it is beyond the scope of this paper to present all the results comparing 247, 410, 485 and 550 static heights simulation results with 300 μm particle size and 0.45 initial voidage, a brief summary is provided here. It seems that the higher the static heights, the lesser the deviation $|e|_{av}$ of bed expansion while the behaviours are similar in which they exhibit close match with experimental data at lower water inflow rates but large deviation at higher rates.

3.3.3. Bed expansion–superficial fluid velocity correlation

The superficial fluid velocity can be derived from the cone dimensions, the fluidized height and the flow rate. From Figs. 17–20, it is evident that the relationship between the superficial water velocity and the bed expansion is independent of static height since most of the data lay closely to the linear model of each set. The relationship between bed expansion and superficial fluid velocity can be used to predict the flow rate and bed expansion characteristics once the dimensions of the container are known.

3.3.4. Voidage–velocity correlation

The voidage and superficial fluid velocity can be described using the Richardson and Zaki equation [11], Eq. (6), by taking logarithmic function for both left and right hand sides, a linear correlation can be produced as shown in Eq. (7) below:

$$\log v_f = n \log \varepsilon + \log v_o \tag{7}$$

From Fig. 21, it is evident that there is a linear correlation with the data according to the Richardson and Zaki correlation since the values lie closely to the linear model of each set. Also, the constant parameter, n can be determined from the slope of linear model of

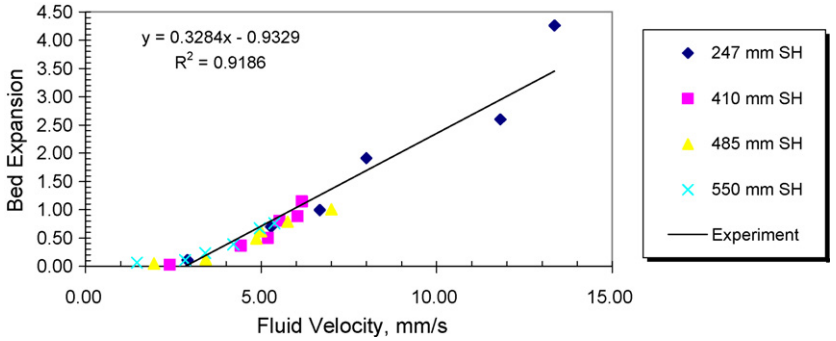

Fig. 18. Bed expansion vs. superficial fluid velocity for simulation model with 300 μm particle size and initial voidage of 0.45 (SH—static height).

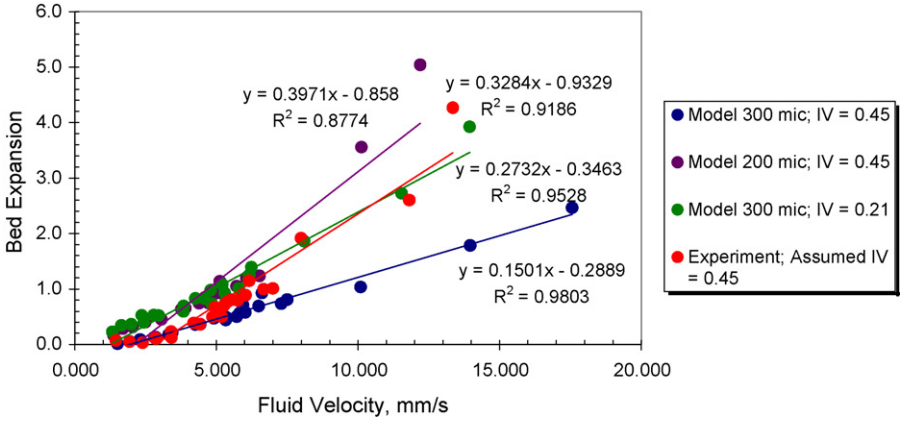

Fig. 19. Combined results for bed expansion vs. superficial fluid velocity comparing experiment and different parameters sets in simulation models.

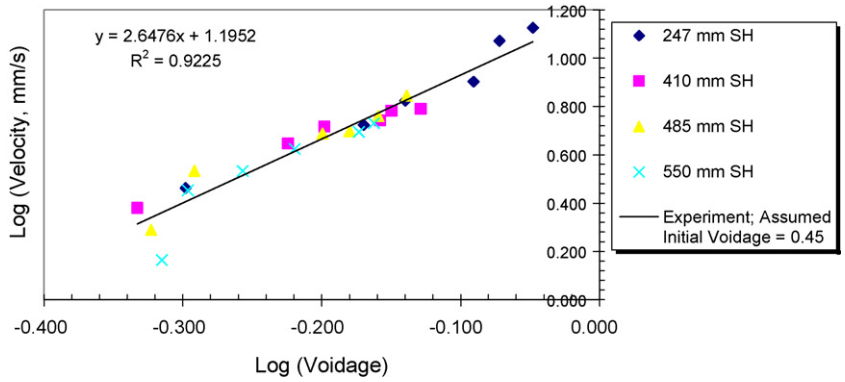

Fig. 20. Log (superficial water velocity) vs. Log (voidage) for experimental result with assumed initial voidage of 0.45 (SH—static height).

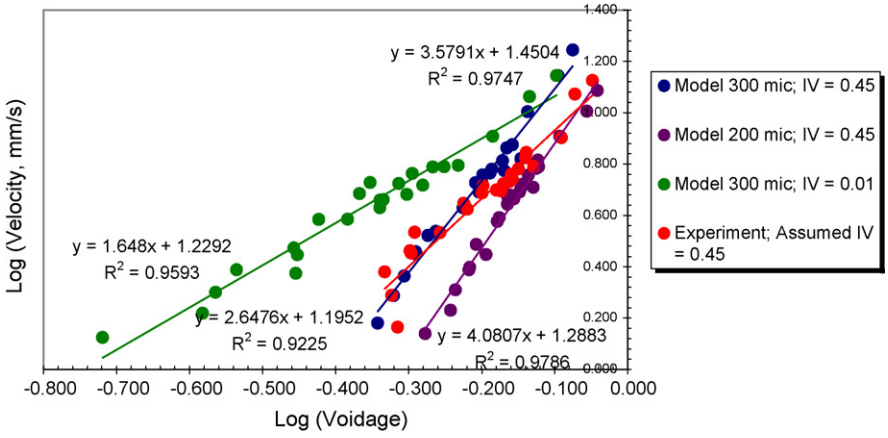

Fig. 21. Combined results for Log (superficial water velocity) vs. Log (voidage) comparing experiment and different parameters set in simulations.

each plot while the constant parameter, v_o can be found from the anti-logarithm of the intercept coefficient of the linear model of each plot.

3.3.5. *Proposed cone simulations*

Dimensions for a proposed commercial cone (Proposed Cone 1, Table 1) were arrived at, based on the scaling-up procedure of multiplying the entire field based cone dimension with four, to achieve a targeted flow rate of 20 L/s. However, in view of constructing the cone commercially, the height of the cone was truncated. Simulations with proposed Cone 1 indicated that a bed expansion of 0.54 is achievable (Fig. 22), which was thought to be an insufficient bed expansion for constructing a commercial size limestone reactor. Hence, a different method was adopted (due to confidentiality the method cannot be outlined here), to modify the dimensions further to achieve increased bed expansion.

Simulations with the modified dimensions (Proposed Cone 2) using the modified method, predicted that the proposed cone could achieve a bed expansion of 0.68 (Fig. 23). Hence, by modifying the cone dimensions using the scale up procedure based on proportionate volumes, it was possible to increase the bed expansion.

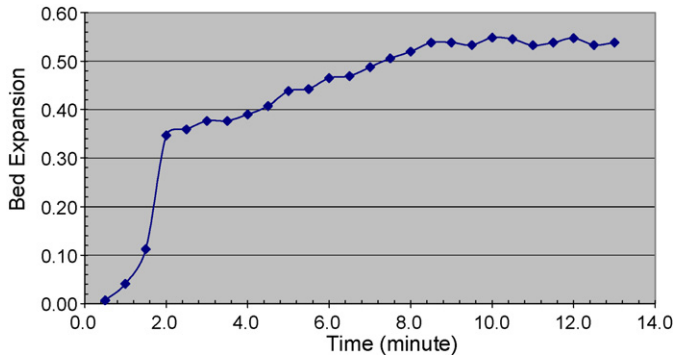

Fig. 22. Bed expansion as a function of time for Proposed Cone 1 with F = 20 L/s, 2.4 m static height, 300 μm particle size and initial voidage of 0.45.

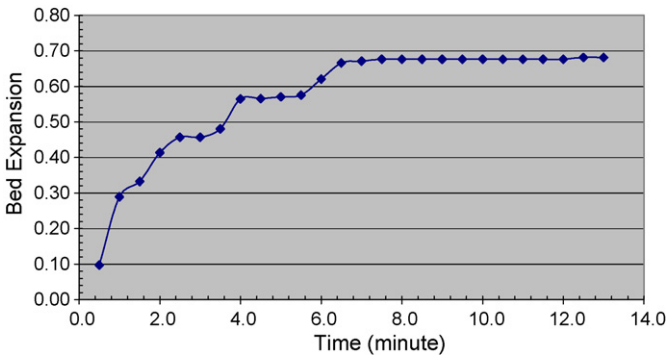

Fig. 23. Bed expansion as a function of time for Proposed Cone 2 with F = 20 L/s, 2.52 m static height, 300 μm particle size and initial voidage of 0.45.

However, the model would need significantly more work if it were to be used with confidence to design cones of differing dimensions.

4. Conclusion

The results showed that CFD is a powerful tool to investigate the behaviour of fluidization of limestone within the conical FLRs. The model achieved its purpose of testing different cones to arrive at a commercial size FLR design. According to the new proposed cone (Proposed Cone 2) simulations, the bed expansion in a 20 L/s cone will be 0.68, which is in line with the anticipated bed expansion. However, the model requires further refinement if it is to be used with confidence to design cones of differing dimensions. It is recommended that different cones designed by scaling-up, based on proportional increases in cone dimensions, need to be simulated in a systematic manner so as to arrive at a generic procedure to up-scale any FLR. The present approach of designing by scaling-up based on volumes was followed in view of practical difficulties associated with the construction of a commercial size limestone reactor. An improved understanding of the fluid dynamics was achieved through the development of a CFD model that simulates particle movement within the fluidized limestone reactor.

Acknowledgement

The authors wish to thank The Australian Coal Industry's Research Program (ACARP) for providing the financial support to carry out this collaborative research work.

Appendix A

The bed expansion, B and superficial fluid velocity at the observed fluidized height, v_f are calculated based on the following equation:

$$B = \frac{V_f - V_s}{V_s}$$

where

$$V_f = \frac{\pi h_f[(d_f/2)^2 + (d_f/2)(d_b/2) + (d_b/2)^2]}{3} - \frac{(h_f - h_g)\pi d_t^2}{4}$$

$$V_s = \frac{\pi h_s[(d_s/2)^2 + (d_s/2)(d_s/2) + (d_b/2)^2]}{3} - \frac{(h_s - h_g)\pi d_t^2 v_f}{4}$$

$$= F\pi\left(\frac{d_f^2}{4} - \frac{d_t^2}{4}\right)$$

V_f is the fluidized volume (m^3), V_s the static volume (m^3), d_f the fluidized diameter, diameter measured at the top of the fluidized aggregate bed (m), d_s the static diameter, diameter measured at the top of the static aggregate bed, under conditions of no water flow (m), d_b the base diameter, diameter measured at the base of the truncated cone (m), d_t the tube diameter, diameter of water inflow tube (m), h_f the fluidized height, height measured from the top of the fluidized aggregate bed to the base of the truncated cone (m), h_s the static height, height measured from the top of the aggregate bed to the base of the truncated cone (m), h_g the gap between inflow tube and the base of the truncated cone (m), and F is the inflow rates of water.

Appendix B. Supplementary data

Supplementary data associated with this article can be found, in the online version, at doi:10.1016/j.cej.2008.10.014.

References

[1] D.E. Arnold, Diversion wells—a low cost approach to treatment of acid mine drainage, in: Proceedings of the Twelfth Annual West Virginia Surface Mine Drainage Task Force Symposium, Morgantown, West Virginia, April 1991, pp. 3–4.
[2] J.E. Fraser, et al., Acid Precipitation Mitigation Program Guidance Manual, vol. II: Liming materials and methods, Biological Report 80 (40.25), U.S. Fish and Wildlife Service, Leetown, W. Virginia, 1985.
[3] J.P. Maree, G.J. Van Tonder, P. Millard, T.C. Erasmus, Pilot-scale neutralisation of underground mine water, Water Sci. Technol. 34 (10) (1996) 141–149.
[4] J.P. Maree, G.J. van Tonder, P. Millard, T.C. Erasmus, Underground neutralisation of mine water with limestone, Water Sewage Effluent 16 (3) (1996) 21–23.
[5] J.P. Maree, M.J. Hagger, G. Strobos, P. Hlabela, H. Cronje, A. Van Niekerk, A. Wurster, R. Nengovhela, F.B. Waanders, Design criteria for limestone neutralization at a nickel mine, Mine Water Environ. 23 (2004) 152–156.
[6] Philip L. Sibrell, Jane M. Hammarstrom, Harvey E. Belkin, Characterization of limestone reacted with acid-mine drainage in a pulsed limestone bed treatment system at the Friendship Hill National Historical Site, Pennsylvania, USA, Appl. Geochem. 18 (November (11)) (2003) 1705–1721.
[7] Barnaby J. Watten, Philip L. Sibrell, Michael F. Schwartz, Acid neutralization within limestone sand reactors receiving coal mine drainage, Environ. Pollut. 137 (September (2)) (2005) 295–304.
[8] M. Rhodes, Introduction to Particle Technology, John Wiley & Sons Ltd., Chichester, 1998.
[9] S. Ergun, Fluid flow through packed columns, Chem. Eng. Prog. 48 (2) (1952) 89–94.
[10] C.Y. Wen, Y.H. Yu, Mechanics of fluidization, Chem. Eng. Prog. Symp. Series 62 (1966) 100–111.
[11] J.R. Richardson, W.N. Zaki, Sedimentation and fluidization: part I, Trans. Inst. Chem. Eng. 32 (1954) 35–53.
[12] W. Du, X. BAO, J. Xu, Computational fluid dynamics (CFD) modelling of spouted bed: assessment of drag coefficient correlations, Chem. Eng. Sci. 61 (5) (2006) 1401–1420.
[13] S. Roy, M.P. Dudukovic, Flow mapping and modelling of liquid–solid risers, Ind. Eng. Chem. Res. 40 (2001) 5440–5454.
[14] Y. Cheng, J.X. Zhu, CFD modelling and simulation of hydrodynamics in liquid–solid circulating fluidised bed, Can. J. Chem. Eng. 83 (2005) 177–185.
[15] E. Doroodchi, K.P. Galvina, D.F. Fletcherb, The influence of inclined plates on expansion behaviour of solid suspensions in a liquid fluidised bed—a computational fluid dynamics study, Powder Technol. 160 (2005) 20–26.
[16] R. Panneerselvam, S. Savithri, G.D. Surender, CFD based investigations on hydrodynamics and energy dissipation due to solid motion in liquid fluidised bed, Chem. Eng. J. 132 (2007) 159–171.
[17] Jack T. Cornelissen, Fariborz Taghipour, Renaud Escudié, Naoko Ellis, John R. Grace, CFD modelling of a liquid–solid fluidized bed, Chem. Eng. Sci. 62 (2007) 6334–6348.
[18] J.A. Yasuna, H.R. Moyer, S. Elliott, J.L. Sinclair, Quantitative predictions of gas-particle flow in a vertical pipe with particle–particle interactions, Powder Technol. 84 (1) (1995) 23–34.
[19] M. Syamlal, T.J. O'Brien, Computer simulation of bubbles in a fluidized bed, AIChE Symp. Series 85 (1989) 22–31.
[20] H. Enwald, E. Peirano, A.-E. Almstedt, Eulerian two-phase flow theory applied to fluidization, Int. J. Multiphase Flow 22 (1996) 21–66.
[21] B.G.M. Van Wachem, J. van der Schaaf, J.C. Schouten, R. Krishna, C.M. van den Bleek, Experimental validation of Lagrangian–Eulerian simulations of fluidized beds, Powder Technol. 116 (2–3) (2001) 155–165.
[22] S.S. Thakre, J.B. Joshi, CFD simulation of bubble column reactors: importance of drag force formulation, Chem. Eng. Sci. 54 (November (21)) (1999) 5055–5060.
[23] D. Gidaspow, R. Bezburuah, J. Ding, Hydrodynamics of circulating fluidized beds, kinetic theory approach, in: Fluidization VII, Proceedings of the 7th Engineering Foundation Conference on Fluidization, 1992, pp. 75–82.
[24] Fluent 6.0 Tutorial 19 2001, Using the Eulerian Multiphase Model for Granular Flow, Fluent Inc.
[25] (a) J.M. Dalla Valle, Micromeritics, Pittman, London, 1948;
(b) J. Ding, D. Gidaspow, A bubbling fluidization model using kinetic theory of granular flow, AIChE J. 36 (4) (1990) 523–538.
[26] J. Garside, M.R. Al-Dibouni, Velocity–voidage relationships for fluidization and sedimentation, I & EC Process Des. Dev. 16 (1977) 206–214.
[27] D. Gidaspow, H. Lu, A comparison of gas–solid and liquid–solid fluidization using kinetic theory and statistical mechanics, in: L.-S. Fan, T.M. Knowlton (Eds.), Fluidization IX, Engineering Foundation, New York, 1998, pp. 661–668.